EasyChair Preprint

№ 8083

Observation of Diffraction from Absorber Array and Field-Probe Using Long Vertical Objects

Pax Wei

EasyChair preprints are intended for rapid dissemination of research results and are integrated with the rest of EasyChair.

May 24, 2022

Observation of diffraction from absorber array and field-probe using long vertical objects

P. S. P. Wei ** (retired)
The Boeing Company, Seattle, Washington

Abstract: A compact range lined with rows of absorbers on all sides would offer a unique opportunity for the curious mind to study its diffraction effect even under very dim illumination [1]. An extended long object usually gives rise to a bright reflection (glint) when viewed near its surface normal. To take advantage of this phenomenon, a discrete Fourier transform (DFT) on RCS measurements would yield a spectrum of incident wave distribution along that object [2]. Some interesting physics are discussed.

Keywords: RCS measurements, compact range, absorber array, diffraction, field probes, extended long objects

1. The Boeing 9-77 compact range

The Boeing 9-77 indoor compact range was constructed in 1988 based on the largest Harris model 1640. Figure 1 is a schematic view of the chamber, which is of the Cassegranian configuration with dual-reflectors. The relative position of the main reflector and the upper turntable (UTT) are as shown. The inside dimensions of the chamber are 216-ft long, by 80-ft high, and 110-ft wide. For convenience, we define a set of Cartesian coordinates (**x**: pointing out of the paper, **y**: pointing up, **z**: pointing down-range), with the origin at the center of the quiet zone (QZ). The QZ was designed as an ellipsoidal volume of length 50-ft along **z**, height 28-ft along **y**, and width 40-ft along **x**. The back wall is located at **z** = 75 ft, whereas the center of the roll-edged main reflector (tilted at 25^o from vertical) is at **z** = **-**110 ft. It is estimated that the design approach controls the energy by focusing 98% of it inside the QZ for target measurements. The residual field spreading out from the main reflector was attenuated by various absorbers arranged in arrays and covering the chamber walls. The four walls facing the QZ, i.e., the right, left, top and bottom were all covered by the Rantec EHP-26 pyramidal absorbers. A two-by-two unit of it was lifted up for display on the left side in Figure 2. Equipped with strings, the UTT is for lifting a target to the QZ center and maneuvering its yaw, pitch, and roll for measurements. With all other parts being stationary, the angular position of the UTT would affect the empty-chamber background (see Figures 3 and 4). [1]

2. Anechoic chamber

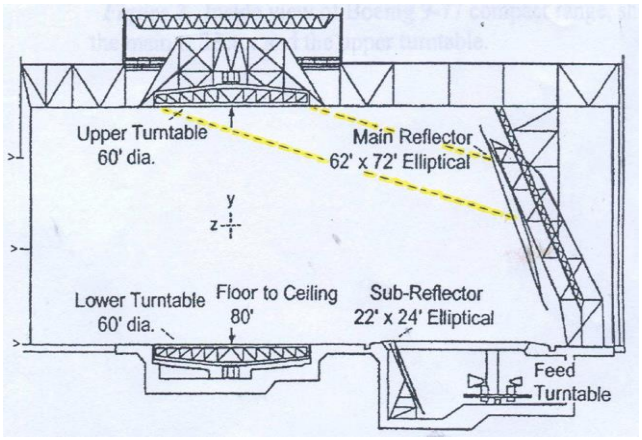

Figure 1. A schematic sideview of the Boeing 9-77 compact range. The dashed lines (yellow) represent an angle 15.26^o from the ceiling in a "blazed grating" condition when the rows are aligned along the z-axis.

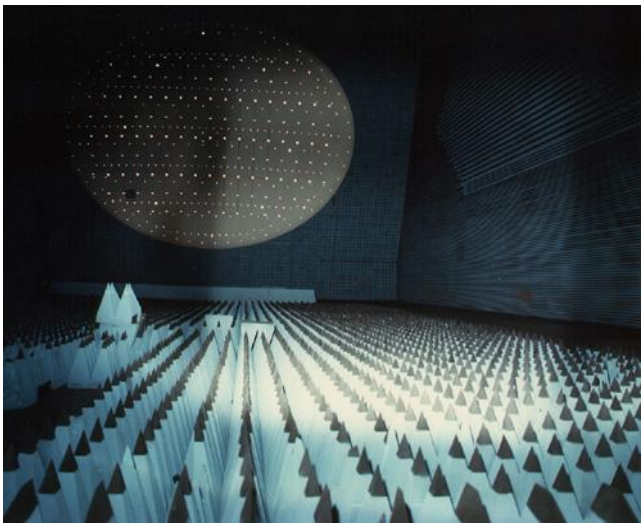

Figure 2. Inside view of the Boeing 9-77 compact range showing the floor covered with pyramidal absorbers in a 1-foot square array. It has a 4-fold symmetry with the tip of a pyramid at 12" apart from its 4 nearest neighbors. The UTT is covered with similar absorbers (see ***Appendix***)

3. Empty-Chamber Background

Summary of empty-chamber background versus azimuth and frequency is shown in Figure 3 for VV and Figure 4 for HH. The results are similar to diffraction patterns. [1]

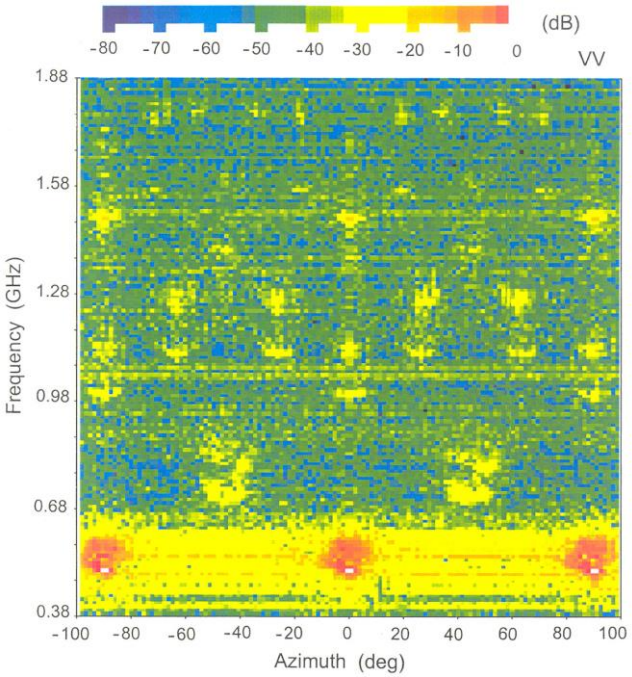

Figure 3. Angular and frequency dependencies of the rotating UTT background in VV. For the 12"-square lattice, there is no Bragg diffraction below 0.50 GHz.

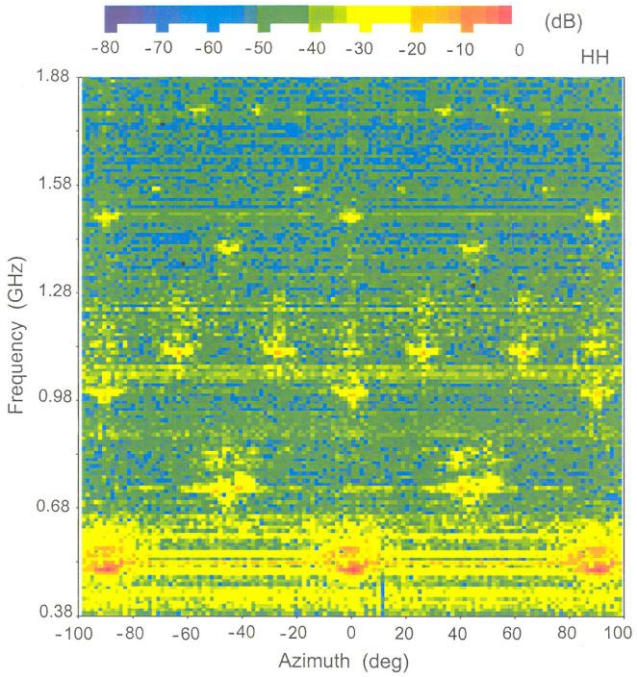

Figure 4. Angular and frequency dependencies of the rotating UTT background in HH, no diffraction $\leq$ 0.5 GHz

4. Imaging of the UTT

The radar data collected as a function of azimuth, frequency, polarization, amplitude and phase, may serve as input for the 2-D DFT algorithm to generate an image on the location of scatters in the scene. The central portions of $\pm$10 ft are shown. With the intensity scale calibrated, we find that the peak intensities are typically –70 dBsm for VV and –75 dBsm for HH. These are recognized as peak contributions from absorbers.

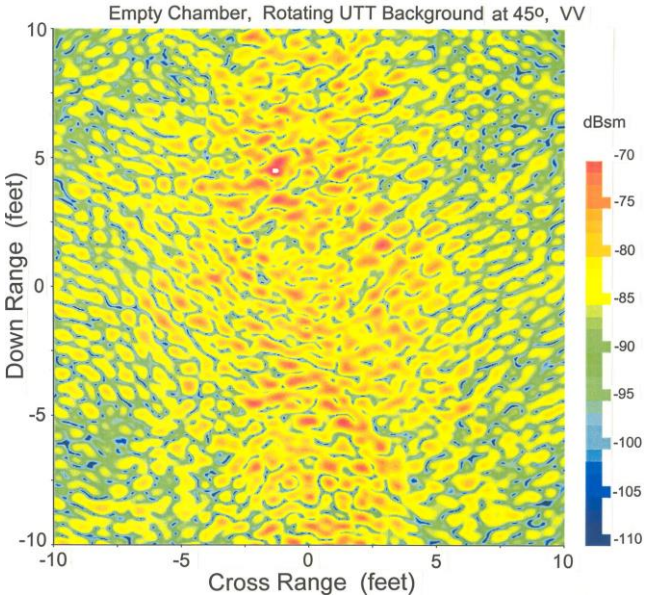

Figure 5. Image of rotating UTT background for VV.

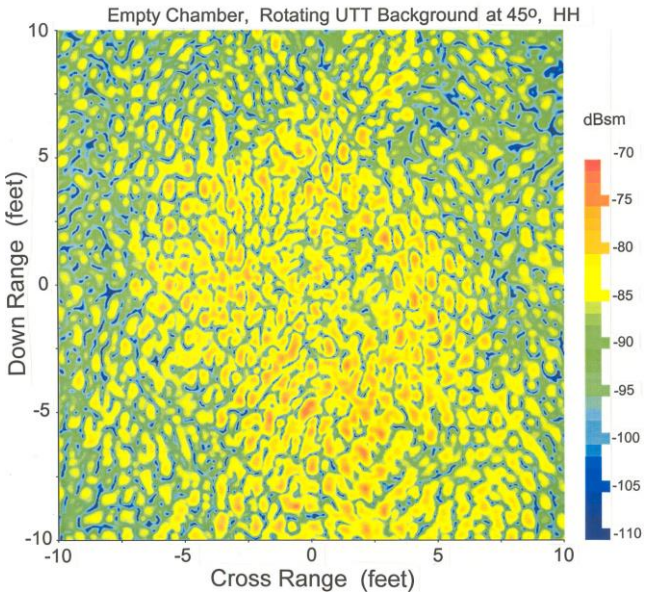

Figure 6. Image of rotating UTT background for HH. The absorber tips at 1-ft apart are almost resolved.

5. Vertical Measurements

Figure 7 shows the configuration for moving an object in a vertical plane using the high-capacity string-reels. [2]

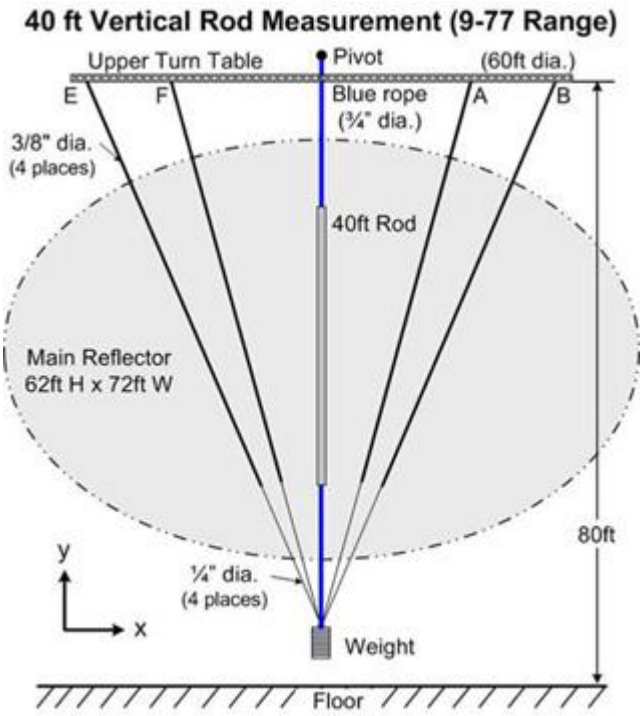

Figure 7. Schematic of the test geometry looking toward the main reflector. Note the Cartesian coordinates (X, Y) as defined. The Z-axis is pointing out from the XY-plane.

The 40-ft aluminum rod (dia. 4-inch) supported by a blue rope through its center was the first target measured. The angular motion of the rod with respect to the pivot (on top) was achieved by pulling on the weight either by the pair of strings A & F from the front side, or by the pair of strings B & E from the back side. The RCS data thus collected as a function of the translation distance of the lower end of rod along Z (proportional to the out-of-plane tilt angle) were studied and analyzed. The second target was a separate piece of blue rope (dielectric, of dia. 0.75-inch before stretched).

Figures 8 and 9 show, respectively, the measured radar echoes at 2.4 GHz on the 40-ft rod and on the long blue rope. They looked very similar, except in [dBsm] scales. In Figure 9, the difference in peak RCS for the blue rope, (VV-HH) at 2.4 GHz, was found to be 6.002 dB. With reference to the wave equations for thin dielectric strings, the ratio of $(T_E / T_H)^2$ of the vertical string gives rise to a simple expression of $\{(\varepsilon_o+1)^2 / 4\}$, where $\varepsilon_o = 2.99$ can be estimated as the dielectric constant of the rope [2].

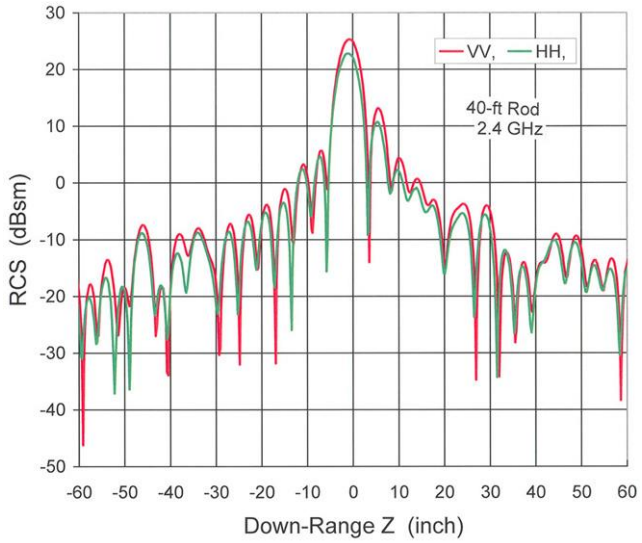

Figure 8. Radar responses from the vertical 40-ft rod at 2.4 GHz versus distance Z. The pattern reached its peak within a narrow range in Z when the rod was at broadside to the wave-front.

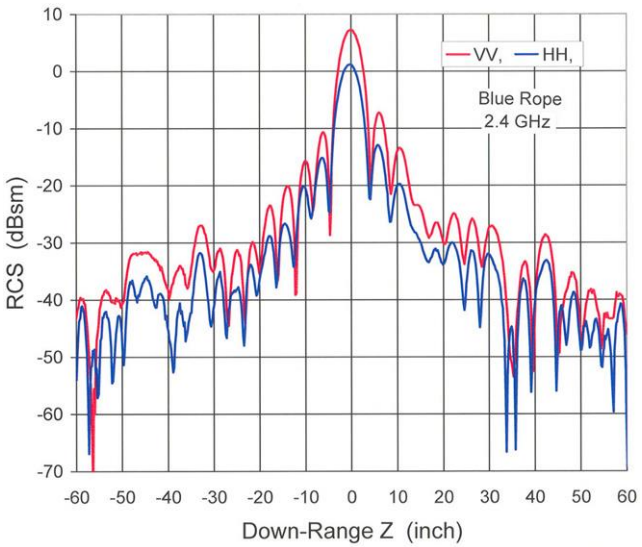

Figure 9. Radar responses from the vertical blue rope at 2.4 GHz versus distance Z. Though similar to Fig. 8 above, the HH scattering from the dielectric rope was weaker than its VV by 6 dB.

Also in Figure 9, the peak RCS for the rope in VV at 2.4 GHz was measured at 7.124 [dBsm]. Though the ka value at 0.479 (for the original radius of 0.375 inch) was moderate, not thin, let us assume that the equation for $S_{vv} = (T_E)^2 = [(L / 2) (\pi)^{1/2} (\varepsilon_o-1) (ka)^2]^2$ may still apply [2]. By using L = 11.486 meter, and $\varepsilon_o = 2.99$, we can estimate the ka to be 0.335, or a = 0.262 inch as the "effective" radius of the rope (for wave scattering) after being stretched under a heavy weight.

6. Field probe along the vertical objects

The raw data measured for Figures 8 & 9 were not equally spaced. In order to apply DFT, we used a cubic-spline fit to smooth them. The results of field distribution vs vertical distance for the 40-ft rod and the blue rope are plotted here. They looked very similar except the dBsm scale and the calibrated vertical distance. [2]

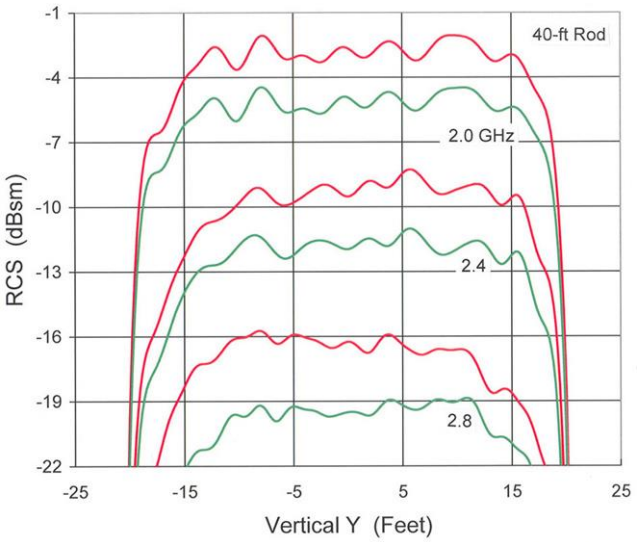

Figure 10. DFT spectra versus vertical distance from the 40-ft rod at selected frequencies and polarization [VV (red) and HH (green)]. The cutoffs were due to the finite length of the rod.

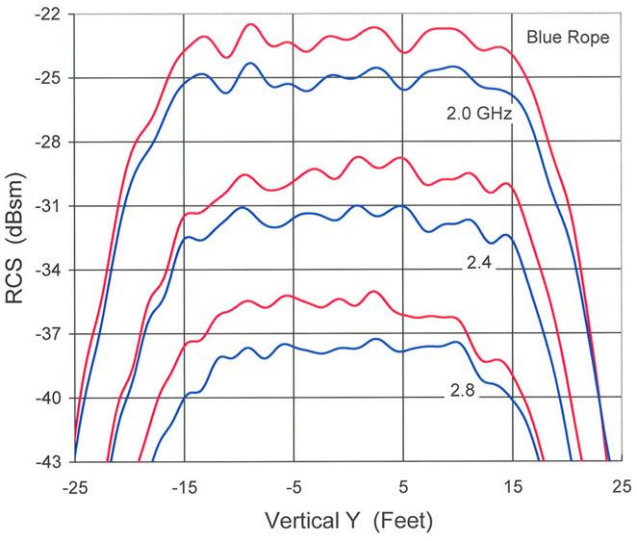

Figure 11. DFT spectra from the blue rope versus frequency and polarization [VV (red) and HH (blue)]. The results showed a wider field distribution tapered out from the quiet zone boundary. Except different in RCS scale (dBsm) for the two vertical objects, the features of Figures 10 and 11 (as representation of field distribution) looked extremely similar, per frequency, and per polarization.

For comparison with the new results shown in Figures 10 and 11, we re-visit the field probes measured by translating a sphere supported by strings in the vertical direction through the quiet zone center, (data collected in 1996). In Figure 12 (plotted with the same scales), we see that the field distributions are very comparable with the new results, except that a long object senses a wider distance.

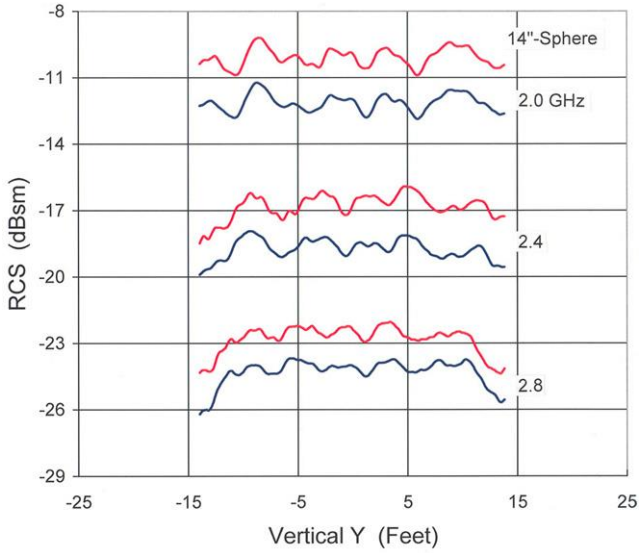

Figure 12. Vertical field probes by a calibration sphere versus frequency and polarization recorded in 1996. The quiet zone boundary in the vertical dimension was specified as ± 14 ft, (or ± 168 inches).

7. Summary and Conclusion

Observing the diffraction effect from the regularly arranged absorbers in the anechoic chamber was a dream come true. Imaging the very low RCS of the absorber tip was a bonus. We conclude that the new method of conducting field probe by the angular motion of a long rigid object (in either the horizontal [3] or vertical plane) has been demonstrated and validated. Further studies should shed new light on RCS research.

--- References ---

[1]. P. S. P. Wei, "Scattering of the residual field above and beyond the quiet zone of a compact range," Proc. 35th AMTA, Columbus, OH (2013).

[2]. P. S. P. Wei, "Measurements on long and rigid objects for radar field probes" Proc. 34th AMTA, pp. 195-200 (2012); Also in ACES Journal 28, 1228-1235 (2013).

[3]. P. S. P. Wei, "Measurements on extended objects for radar field probes," Proc. 41st AMTA, pp. 199-204 (2019); Also presented at ICECOM-2019 (23rd International Conf. on Applied Electromagnetics & Communications), paper s_16_3, Dubrovnik, Croatia, Sept. 30, 2019.

Appendix-1. The Rotating UTT as a 2-D array

When a person first sets foot inside the anechoic chamber, one may pause to admire its enormity. Looking at the regularly arranged "sea" of absorbers as shown in Figure 2, a worker with some knowledge in physics may wonder if diffraction phenomena could be observable, even under the very dim intensity of the residual field. The results presented in Figures 3 to 6 would provide a positive answer to the quest for truth. Putting the VV and HH in the same column would allow easy comparisons on polarization with respect to the empty-chamber background (Figs 3 & 4). The 2-D DFT spectra would show its usefulness in extracting the extremely low RCS contributions from the absorber array tips (Figs 5 & 6).

The UTT (of radius 30-ft) can accommodate 2827 Rantec EHP-26 pyramidal absorbers (each of base-area 1 sq-ft, 4"-thick, with four inclined surfaces of 22" height) with the downward pointing tips arranged in a simple square lattice of 12" unit cells in the (x, z) plane, at a nominal height of y = 37.83 ft. When the UTT rotates, it brings the various rows parallel to the radar wave-front at specific azimuths. If minor differences are ignored, we find that the square lattice exhibits a four-fold symmetry. For scattering from a 2-D periodic lattice, the Bragg conditions are given by: $2d \sin\theta = m\lambda = mc / F$, or $F = mc / 2d \sin\theta$, where d is the inter-row spacing, θ is the angle from the grating normal, m is an integer, c = speed of light = 11.803 inch/nsec, and F is the frequency in GHz. For wavelength λ longer that d, or $F \leq 0.5$ GHz, there is no diffraction.

The 4-fold symmetry is analogous to a LEED (low-energy electron diffraction) pattern from the (100) surface of a cubic lattice [4, 5]. Observation of diffraction from a spatial array is equivalent to mapping in the ***reciprocal space*** (the ***k***-space). The reciprocal lattice of a 2-D square lattice is also a square lattice with the same azimuth angle. The (1, 0) beam would occur at 0° degree and 0.495 GHz, whereas the (1, 1) beam would occur at 45° and 0.696 GHz. These are in good agreement with the observed patterns in Fig's 3 & 4. Higher ordered beams have been observed up to ~4 GHz. Above ~4 GHz, the diffraction contribution blends into the general background.

In optics, when the facet normal of a grating becomes parallel to the direction of reflection, the diffracted beam intensity will be greatly enhanced, called a ***blazed grating*** condition [6]. In the present case, it would happen 4 times per revolution of the UTT, whenever the rows of absorbers are all aligned parallel to the z-axis. All absorber tips would project toward the main reflector within an ellipse (of 60-ft long by 19-ft height) as shown in Figure A1.

In Figures 3 and 4, the azimuth data in steps of 1.53°, are plotted from -100° to 100° for a total of 131 pixels. Note

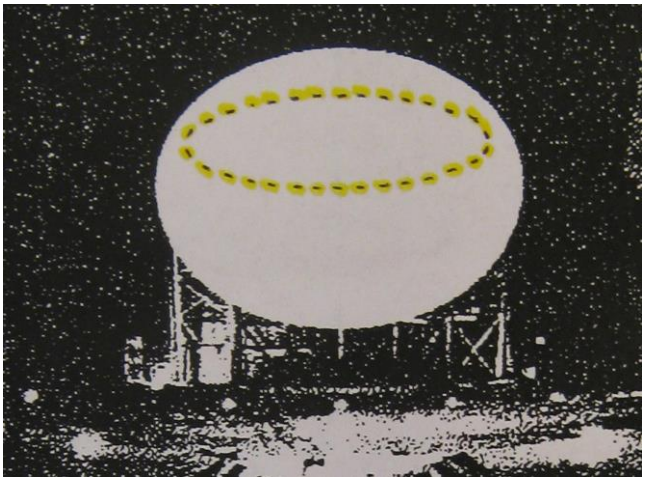

Figure A1. Projected ellipse from the surface-normal of all the pyramidal tips on the UTT to the main reflector, which is analogous to the "***blazed grating***" condition in optics [6].

that the ellipse moves off from the main reflector in merely one pixel of 1.53°. The frequency spans three bands from 0.38 to 1.88 GHz, in steps of 0.01, for a total of 151 pixels. Though finer steps are possible, we find that the present choices are optimum for resolving the diffraction feature.

The most prominent (1, 0) beam occurs at 0.495 GHz and 0° degree, and again by symmetry at $\pm 90^{\circ}$. Of particular interest are the 2 pixels of the highest intensity (appearing as ***white*** in Fig. 3 for VV, and as ***red*** in Fig. 4 for HH). In addition, the neighboring pixels within an azimuth of $\pm 10^{\circ}$ and frequency from 0.50 to 0.59 GHz all exhibit a high intensity. This may be understood as due to the large size of the main reflector, which simultaneously serves as the transmitter and the receiver. Unlike a point source, incident (and diffracted) angles in the vertical yz-plane from 55° to 86° are all possible. For a given diffracted beam to occur, the frequency F is inversely proportional to $\sin\theta$. For θ from 55° to 86°, $1/\sin\theta = 1.22$ to 1.002. Hence, a broadened spot for the (1, 0) beam can be expected. The (1, 1) beam with its onset at 45° and 0.696 GHz exhibits an interesting split-appearance in azimuth and frequency. It turns out that at that angle the radar wave senses the ridges of the pyramidal absorber rather than the flat surface. More details may be found in [1].

--- References (2) ---

[4]. L. H. Germer, "The structure of crystal surfaces," Scientific Am., vol. 212, No. 3, March pp. 32-41 (1965).

[5]. C. Kittel, "Introduction to Solid State Physics," (Wiley, 1968), pp. 35-38 (LEED), & p. 54, reciprocal lattice in 2-dimensions.

[6]. M. Born and E. Wolf, "Principles of optics," (Pergamon Press, 3rd ed., 1965), page 409.

Appendix-2. About RCS Measurements

Due to the original limit of 4 pages, much wording has been omitted to save space for the 12 figures which describe the *title story*. Per Reviewer's suggestions, Appendix-1 & -2 are hereby added for a better reading.

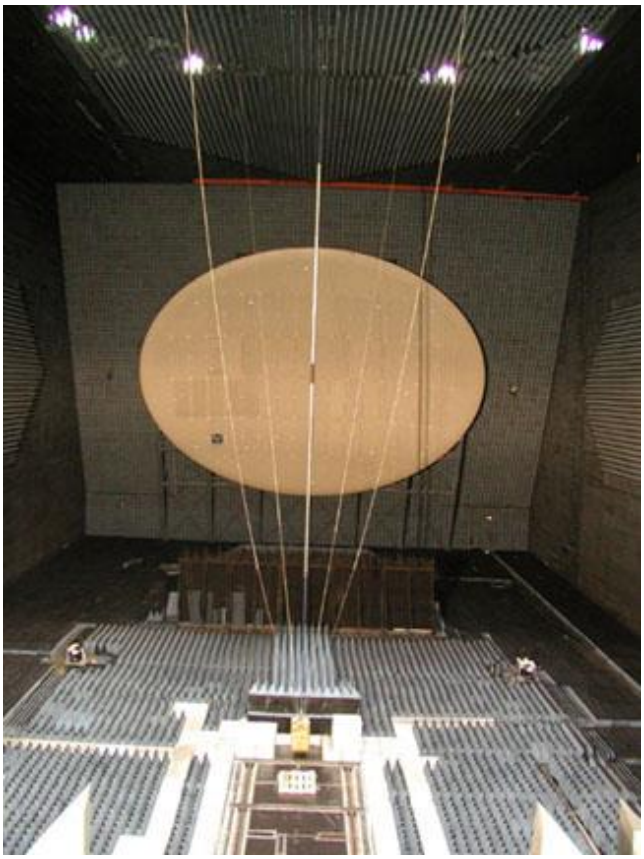

Fig. A2. A photograph of the test geometry for vertical measurements as viewed from the back (related to Fig. 7). The lights around the rim of the 60-ft UTT are visible on top. A heavy weight is suspended near the floor.

Figs 8 and 9 show the measured radar echoes at 2.4 GHz from the 40-ft rod and the long blue rope, respectively. They look very similar, except in [dBsm] scales [2]. The RCS measurements as a function of the lower-end distance along the z-axis (out-of-paper) are like diffraction patterns from the long objects. The **amplitude** (intensity in dBsm) is merely half of the data, with the **phase** being inherent but not plotted.

From the simple test geometry shown above, it would be quite difficult to move the long-object in equal steps as required for the DFT application. As a remedy, we've tried a 2-point **linear** averaging method, as well as a 4-point **cubic-spline** interpolation to re-sample the data in equal steps, with the latter being better and more realistic. [2]

Figs 10 and 11 show the DFT spectra for the 40-ft rod and the blue rope, respectively, at three S-band frequencies for both VV and HH. For easy comparison, these are plotted at the same scales, commonly known as the range profiles. An important finding is the cut-off at $\pm$20 ft for the 40-ft rod in Fig. 10. Yet, in Fig.11 the blue-rope of length 70-ft would show responses extending beyond (or outside of) $\pm$20 ft. The extremely similar wiggles in Figs 10 and 11 are recognized as field distributions, per frequency and per polarization. This is due to the long objects being of uniform scattering property, whether they be metallic or dielectric.

The DFT results described above, though derived from the equally stepped complex amplitude-&-phase data from those of Figs 8 & 9, cannot be directly discerned by just intuitively looking at the plots of Figs 8 & 9 alone. It demonstrates the powerful capability of DFT to extract the hidden features from the RCS data.

Previously, when a 60-ft long rod suspended horizontally by the UTT and rotated at constant speed through a small angle about its broadside, the RCS data were naturally equally spaced. The DFT spectra would represent a **horizontal** field probe [3]. Thus, the present result of a **vertical** field-probe is complementary to it.

It is interesting to find that the peak intensities encountered in the measurements for Figs 5 & 6 (very weak) to Figs 8 & 9 (strong) would span 9 orders of [dBsm]. The present work has been part of the effort to characterize and calibrate the 9-77 indoor compact range.

Note: In the autumn of 1991, I was assigned to work at the Boeing 9-77 Compact Range in Seattle by Hudson Burke, sharing an office cubical with Eugene Knott. That was my first encounter with the great teacher of RCS measurements. Although the usual task at hand might be dull and routine, his insight and rich experience, plus humor and wit, would often enlighten it to a higher level. The three-month duration was short, but the RCS textbook by Knott, Shaeffer, and Tuley [7] was sufficient to introduce me to much of the working knowledge of its science, engineering, and art [8]. We maintained our friendship and mutual interest on technical matters for the next 23 years [9].

[7]. E. F. Knott, J. F. Shaeffer, and M. T. Tuley, "Radar Cross Section," (Artech House, Boston, 2nd ed., 1993).

[8]. E. F. Knott, "Radar Cross Section Measurements," (Van Nostrand Reinhold, New York, 1993),

[9]. *In Memoriam: Eugene Knott*, IEEE Ant. & Prop. Mag., 56, No. 3, pp. 132-133 (June 2014), by Sam Wei.